



Comparison of quantum cascade structures for detection of nitric oxide at $\sim 5.2 \mu\text{m}$

Andrzej Kolek¹ · Grzegorz Hałdaś¹ · Maciej Bugajski²

Received: 23 August 2019 / Accepted: 19 September 2019 / Published online: 24 September 2019
© The Author(s) 2019

Abstract

Nonequilibrium Green's function method is used to calculate electronic and optical characteristics of various quantum cascade structures emitting light at $\sim 5.2 \mu\text{m}$ wavelength. Basing on these simulations, the choice of optimal design can be done.

Keywords Nonequilibrium Green's function · Quantum cascade laser · Electronic transport · Optical gain · Electron–photon selfenergy

1 Introduction

The design of quantum structures utilized in modern optoelectronic devices is crucial for their performance. The latter, obviously, depends on the evaluation criteria; however, even if these criteria are well established, the choice of optimally designed structure is not easy because devices that use nominally the same structure very often exhibit quite different experimental characteristics. Mostly, this is due to technology/device processing-dependent factors, like leakage or serial resistance, which still contribute much to the final device characteristics and influence them in unpredictable manner. There are also factors, like, e.g., doping level, which are different in individual devices, but influence device characteristics in complex, not fully recognized way, so that bringing them to some reference point (in order to make the comparison) is hardly possible. Due to these limitations, the evaluation of quantum structures in terms of their ability to effectively absorb or gain the light basing exclusively on experimental data appears as a big challenge. For these purposes, numerical simulations seem to be helpful, because they are able to provide data that can be exclusively related to the design of quantum structures responsible for light generation/

✉ Andrzej Kolek
akoleknd@prz.edu.pl
Grzegorz Hałdaś
ghaldas@prz.edu.pl
Maciej Bugajski
bugajski@ite.waw.pl

¹ Department of Electronics Fundamentals, Rzeszow University of Technology, al. Powstańców Warszawy 12, 35-959 Rzeszow, Poland

² Institute of Electron Technology, al. Lotników 32/46, 02-668 Warsaw, Poland

absorption, and so can be used for their evaluation. The condition that must be fulfilled to assure this conjecture is that proper simulation method is used and quantum structure is modeled with sufficient accuracy. Due to these requirements, the methods of quantum device simulation are being brought to the level enabling the calculations of device characteristics with the quantitative accuracy (Lake et al. 1997; Birner et al. 2007; Aeberhard and Morf 2008; Klimeck and Luisier 2008; Klimeck et al. 2008; Kubis et al. 2009; Terazzi and Faist 2010; Hałdaś et al. 2011; Steiger et al. 2011; Kolek et al. 2012; Jirauschek and Kubis 2014; Grange 2015; Jonasson et al. 2016). One of them is nonequilibrium Green's function (NEGF) formalism (Lake et al. 1997; Kubis et al. 2009) which is used in this paper to compare quantum cascade structures emitting light at $\sim 5.2 \mu\text{m}$ wavelength. These structures receive much interest due to their use in NO detection systems (Bakhirkin et al. 2004; Kluczynski et al. 2011), important in numerous applications: health, environment protection, security, and defense are a few to mention. The use of NEGF method to achieve a valuable result is almost a must because in this method coherent phenomena, like quantum tunneling, are simultaneously included with the scattering processes that break phase coherence. Then, the phase-breaking time does not need to be arbitrary assumed or speculated from other considerations but, instead, appears inherently as a result of the interplay between coherent and incoherent phenomena. Quantities, which depend on this time, e.g., the broadening of gain/absorption peak, are then reasonable estimated basing on physical background.

In the following, some details of the model and method used in calculations are briefly described. Then, the results of the simulations made for 4 quantum structures used in $5.2 \mu\text{m}$ quantum cascade lasers (QCLs) are presented, demonstrating that with this approach the selection of the best structure is possible.

2 Model and method

QCLs are unipolar, n-type devices, so the single-band effective-mass Hamiltonian provides a sufficient description. In this Hamiltonian, the influence of valence band can be included assuming that the effective mass of the particle depends on its total energy E . The linear form $m(E) = m^*[1 + (E - E_c)/E_g]$ was assumed for this dependence with the values of the parameters: m^* and E_g evaluated from tight binding sp³d⁵s* model of the band structure of the constituents building the QCL device (Kato and Souma 2019). Conduction bandgap offsets between these constituents were calculated basing on model-solid theory including strain (Van de Walle 1989) and material parameters taken from Vurgaftman et al.'s (2001) paper. This method was also used to evaluate bandgap offsets (0.42 eV for InGaAs and 1.53 eV for InAlAs) used in the parametrization of alloy disorder scattering. The values of the parameters used in the simulations are gathered in Table 1.

Table 1 Parameters used in the simulations

Structure	Effective mass/bandgap (eV)		
	Barrier	Well	Bandoffset
E	0.045/0.835	0.091/1.84	0.825
D	0.043/0.808	0.085/1.72	0.670
C	0.045/0.84	0.091/1.82	0.820
K	0.044/0.826	0.092/1.865	0.839

The stratified structure of QCLs allows to simplify the device Hamiltonian to 1D equation in the growth (z) direction with in-plane kinetic energy term $\hbar^2 k^2/2m(E, z)$, where $k = |\mathbf{k}|$ is the magnitude of the in-plane momentum \mathbf{k} . In all, the Hamiltonian used in the simulations reads

$$H = \frac{-\hbar^2}{2} \frac{d}{dz} \frac{1}{m(E, z)} \frac{d}{dz} + V(z) + \frac{\hbar^2 k^2}{m(E, z)}, \quad (1)$$

where the potential $V(z)$ includes the variation of the conduction band edge $E_c(z)$ and the mean field part calculated by solving the Poisson equation.

The calculations were made in the position basis: the base vectors were defined by the points discretizing the device Hamiltonian at certain, nonuniformly distributed z -axis positions. As QCL core is periodic, the structure subjected to the calculations was limited to a bit more than one QCL period connected to the leads that reliably imitated device periodicity (Kubis et al. 2009; Hałdaś et al. 2011). The boundary conditions for the Poisson equation were such that the charge neutrality of each period was preserved and simultaneously the potential difference on the distance of one period equals the applied bias, $V(z) - V(z + d) = eU$, where U is the applied bias and d is the period length. The scatterings occurring in the device were included in the form of appropriate selfenergies incorporated into NEGF equations. The formulations for scattering selfenergies for LO-phonon, interface roughness (IR), ionized impurity and alloy disorder scatterings were taken from Lake et al.'s (1997) paper. For the acoustic (LA) phonons, the approximation of Kubis et al. (2009) was used. For electron–photon interaction, the selfenergies were calculated as in Kolek's (2019) paper using low-density approximation. The equations of NEGF formalism were solved for the steady state. Then, the gain/absorption was calculated basing on the theory outlined by Lee and Wacker (2002), implemented for the case of energy-dependent effective mass (Kolek 2015). All the formulations were adapted for the case of nonuniform grid as in Hałdaś's (2019) paper.

3 Results

Calculations were made for 4 quantum cascade structures used in the devices that emit infrared radiation at $\sim 5.2 \mu\text{m}$ wavelength. Details of these structures can be found respectively in Evans et al.'s (2006) paper for structure E, in Diehl et al.'s (2006) paper for structure D, in Cendejas et al.'s (2011) paper for structure C, and in Kapsalidis et al.'s (2018) paper for structure K. The comparison was done at near-room temperature of 288 K. It was also assumed that the devices have the same number of periods, $N_p = 30$, and were doped to the same sheet density ($n_{\text{dop}} = 0.89 \times 10^{11} \text{ cm}^{-2}$ per period). However, the different doping profiles proposed by the structure designers were maintained. The Gaussian correlation function with the identical interface roughness $\Delta = 0.19 \text{ nm}$ and the correlation length $\Lambda = 9 \text{ nm}$ was assumed for all structures.

The example results of the simulations of the structure E are shown in Fig. 1. In the left graph, the density of electrons (doe) is shown as a color map together with the lines which correspond to the most important states: upper laser state (grey) and lower laser state (red) resonantly coupled to the doublet of discharging states (green, blue). Apart from these, two high-energy states (brown, pink) are shown of which the lower is partly filled. The red broken-line box shows active wells of this QCL design (4-well double-phonon resonance). The momentum-resolved doe integrated over the active wells region is shown in the right

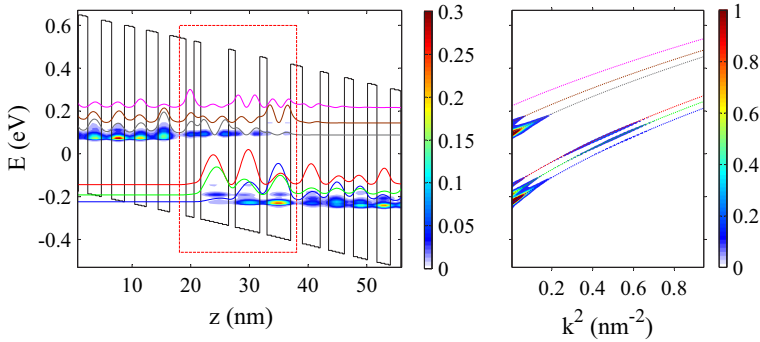


Fig. 1 (left) Density of electrons (color map, unit: $\text{eV}^{-1} \text{nm}^{-1}$) within one period of QCL structure E, biased with the voltage 320 mV/period. Lines show density of states (dos) at energies where dos reaches local maxima within active region of the device (red box). (right) In-plane momentum-resolved doe integrated over the active region (color map, unit: eV^{-1}). Lines show important subbands: the departure from linear dependence is due to the in-plane nonparabolicity included in the device Hamiltonian of Eq. (1). (Color figure online)

graph of Fig. 1. As can be seen, the distribution of electrons in the lower laser states is highly nonthermal. This is because all nonradiative scattering processes can only transfer electrons from upper state to high- k states of the lower subbands. Due to these processes, the bump is formed in the doe in the lower laser subband. This is shown in Fig. 2 which clearly demonstrates that for low photon densities in the cavity the population inversion appears in the low- k states of laser subbands. This inversion, and so the gain, is successively destroyed once the optical field (photon flux) increases.

The evaluation criteria of QCL structures were assumed following the end-users practice. Namely, the parameters like maximum gain, maximum output power or minimum current threshold were compared. For these purposes, the simulations were done for light-matter interaction either included or excluded from the calculations. For the former, the monoenergetic photon flux Φ was increased until the gain at photon energy $E_\gamma, g(E_\gamma, \Phi)$ was clamped to its threshold value, $g_{\text{th}} = 9.5 \text{ cm}^{-1}$. This value corresponds to the overall

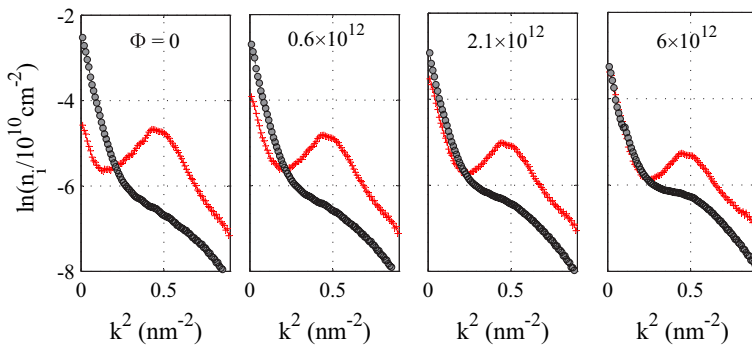


Fig. 2 Evolution of momentum-resolved doe in upper (circles) and lower (crosses) laser subbands of QCL structure E, biased with the voltage 320 mV/period versus photon flux Φ [unit: photons/($\text{nm}^2 \text{s}$)]. For this bias, the threshold gain $g = g_{\text{th}} = 9.5 \text{ cm}^{-1}$ was achieved for $\Phi = \Phi_{\text{th}} = 2.1 \times 10^{12} \text{ photons}/(\text{nm}^2 \text{s})$

Fig. 3 Current–voltage (upper) and gain–current (lower) characteristics calculated for the structures E, D, C, and K with the NEGF method without electron–photon selfenergies. Horizontal line in the lower figure is drawn at the threshold value g_{th}

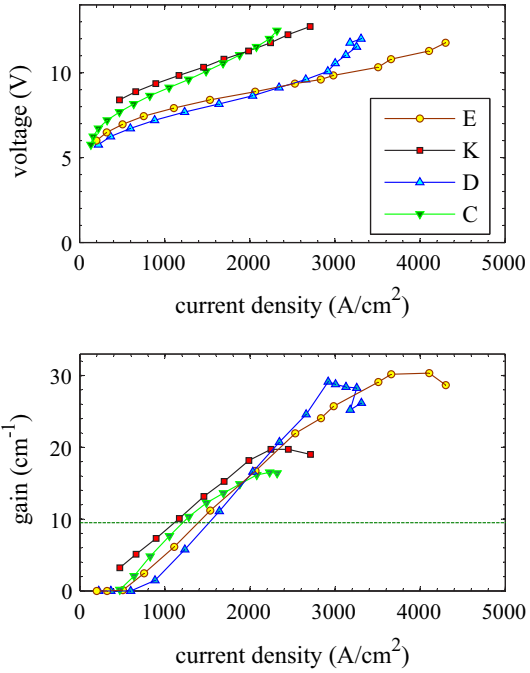
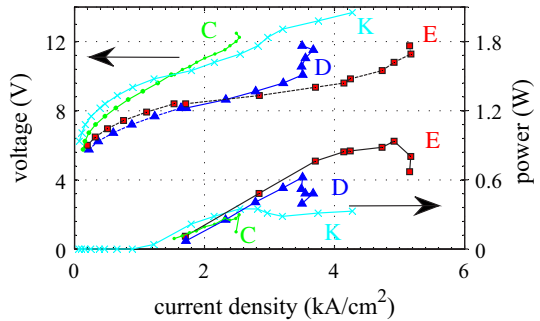


Fig. 4 Current–voltage and light-current characteristics calculated with NEGF method with electron–photon selfenergies



losses in a typical waveguide and was assumed identical for all devices. The photon energy was adjusted to the value E_γ which assures that $g(E_\gamma, \Phi_{th}) = g_{th}$ is the maximum value of the gain spectrum calculated for the threshold flux Φ_{th} . Note that this value not necessarily equals the energy of the gain peak for the field-free conditions. The evolution of laser subbands occupation for the increasing photon flux is presented in Fig. 2. The light power was estimated from Φ_{th} for one facet of $w = 10 \mu\text{m}$ wide cavity as

$$P = (1 - R) N_p dw \Phi_{th} E_\gamma, \tag{2}$$

where $R = 0.27$ is the facet reflectivity.

The results of the simulations, important for structures' evolution, are presented in Figs. 3 and 4. In Fig. 3, the current–voltage and gain–current characteristics are shown for the case without light–matter interaction included in the calculations. The performance parameters read-out from these characteristics are gathered in Table 2: the maximum gain

Table 2 Performance parameters of different QCL structures

Structure	Threshold current (Acm ⁻²)	Gain peak (cm ⁻¹)	Light power (W)
E	1400	30	0.94
D	1550	29	0.61
C	1220	16	0.35
K	1100	20	0.26

of $\sim 30 \text{ cm}^{-1}$ is observed for the structures E and D, whereas the minimum threshold current has the structure K. As can be seen in Fig. 4, the maximum optical power can be achieved in the structure E. This value was estimated from light-current characteristics calculated with electron–photon selfenergies included in the calculations. One can also see that the optical power, available from the structures E and D, differs significantly, even though these structures have almost equal peak values of the zero-field gain. This interesting feature and the underlying physics will be discussed in the upcoming publication.

In summary, the NEGF method was employed to evaluate the performance of different quantum cascade structures used to generate the light of $\sim 5.2 \text{ }\mu\text{m}$ wavelength. This performance depends on the evaluation criteria: the lowest threshold current exhibits the design K of Kapsalidis et al. (2018), while the largest optical power is available for the structure E of Evans et al. (2006). An interesting feature found with the simulation is that the maximum optical power is not exclusively described by the value of the gain peak, but some additional factors mediate this relation.

Acknowledgements This research was supported by the National Centre for Research and Development Grant No. TECHMATSTRATEG1/347510/15/NCBR/2018 (SENSE).

Compliance with ethical standards

Conflict of interest The authors declare that they have no conflict of interest.

Open Access This article is distributed under the terms of the Creative Commons Attribution 4.0 International License (<http://creativecommons.org/licenses/by/4.0/>), which permits unrestricted use, distribution, and reproduction in any medium, provided you give appropriate credit to the original author(s) and the source, provide a link to the Creative Commons license, and indicate if changes were made.

References

- Aeberhard, U., Morf, R.H.: Microscopic nonequilibrium theory of quantum well solar cells. *Phys. Rev. B* **77**(12), 125343 (2008). <https://doi.org/10.1103/PhysRevB.77.125343>
- Bakhrkin, Y.A., Kosterev, A.A., Roller, C., Curl, R.F., Tittel, F.K.: Mid-infrared quantum cascade laser based off-axis integrated cavity output spectroscopy for biogenic nitric oxide detection. *Appl. Opt.* **43**(11), 2257–2266 (2004). <https://doi.org/10.1364/AO.43.002257>
- Birner, S., Zibold, T., Anslauer, T., Kubis, T., Sabathil, M., Trellakis, A., Vogl, P.: nextnano: general purpose 3-D simulations. *IEEE Trans. Electron. Dev.* **54**(9), 2137–2142 (2007). <https://doi.org/10.1109/TED.2007.902871>
- Cendejas, R.A., Liu, Z., Sánchez-Vaynshteyn, W., Caneau, C.G., Zah, Ch., Gmach, C.: Cavity length scaling of quantum cascade lasers for single-mode emission and low heat dissipation, room temperature, continuous wave operation. *IEEE Photonics J.* **3**(1), 71–81 (2011). <https://doi.org/10.1109/JPHOT.2010.2103376>

- Diehl, L., Bour, D., Corzine, S., Zhu, J., Höfler, G., Lončar, M., Troccoli, M., Capasso, F.: High-temperature continuous wave operation of strain-balanced quantum cascade lasers grown by metal organic vapor-phase epitaxy. *Appl. Phys. Lett.* **89**(8), 081101 (2006). <https://doi.org/10.1063/1.2337284>
- Evans, A., Nguyen, J., Slivken, S., Yu, J.S., Darvish, S.R., Razeghi, M.: Quantum-cascade lasers operating in continuous-wave mode above 90 °C at $\Lambda \sim 5.25 \mu\text{m}$. *Appl. Phys. Lett.* **88**(5), 051105 (2006). <https://doi.org/10.1063/1.2171476>
- Grange, T.: Contrasting influence of charged impurities on transport and gain in terahertz quantum cascade lasers. *Phys. Rev. B* **92**(24), 241306 (2015). <https://doi.org/10.1103/PhysRevB.92.241306>
- Haldaš, G.: Implementation of non-uniform mesh in non-equilibrium Green's function simulations of quantum cascade lasers. *J. Comput. Electron.* (2019). <https://doi.org/10.1007/s10825-019-01386-4>
- Haldaš, G., Kolek, A., Tralle, I.: Modeling of mid-infrared quantum cascade laser by means of nonequilibrium Green's functions. *IEEE J. Quantum Electron.* **47**(6), 878–885 (2011). <https://doi.org/10.1109/JQE.2011.2130512>
- Jirauschek, C., Kubis, T.: Modeling techniques for quantum cascade lasers. *Appl. Phys. Rev.* **1**(1), 011307 (2014). <https://doi.org/10.1063/1.4863665>
- Jonasson, O., Mei, S., Karimi, F., Kirch, J., Botez, D., Mawst, L., Knezevic, I.: Quantum transport simulation of high-power 4.6- μm quantum cascade lasers. *Photonics* **3**(2), 38 (2016). <https://doi.org/10.3390/photonics3020038>
- Kapsalidis, F., Shahmohammadi, M., Süess, M.J., Wolf, J.M., Gini, E., Beck, M., Hundt, M., Tuzson, B., Emmenegger, L., Faist, J.: Dual-wavelength DFB quantum cascade lasers: sources for multi-species trace gas spectroscopy. *Appl. Phys. B* **124**(6), 1–17 (2018). <https://doi.org/10.1007/s00340-018-6973-2>
- Kato, T., Souma, S.: Study of an application of non-parabolic complex band structures to the design for mid-infrared quantum cascade lasers. *J. Appl. Phys.* **125**(7), 073101 (2019). <https://doi.org/10.1063/1.5080102>
- Klimeck, G., Luisier, M.: From NEMO1D and NEMO3D to OMEN: moving towards atomistic 3-D quantum transport in nano-scale semiconductors. In: 2008 IEEE International Electron Devices Meeting, pp. 1–4 (2008). <https://doi.org/10.1109/IEDM.2008.4796647>
- Klimeck, G., McLennan, M., Brophy, S.P., Adams III, G.B., Lundstrom, M.S.: nanoHUB.org: advancing education and research in nanotechnology. *Comput. Sci. Eng.* **10**(5), 17–23 (2008). <https://doi.org/10.1109/MCSE.2008.120>
- Kluczynski, P., Lundqvist, S., Westberg, J., Axner, O.: Faraday rotation spectrometer with sub-second response time for detection of nitric oxide using a cw DFB quantum cascade laser at 5.33 μm . *Appl. Phys. B* **103**(2), 451–459 (2011). <https://doi.org/10.1007/s00340-010-4336-8>
- Kolek, A.: Nonequilibrium Green's function formulation of intersubband absorption for nonparabolic single-band effective mass Hamiltonian. *Appl. Phys. Lett.* **106**(18), 181102 (2015). <https://doi.org/10.1063/1.4919762>
- Kolek, A.: Implementation of light-matter interaction in NEGF simulations of QCL. *Opt. Quant. Electron.* **51**(6), 1–9 (2019). <https://doi.org/10.1007/s11082-019-1892-y>
- Kolek, A., Haldaš, G., Bugajski, M.: Nonthermal carrier distributions in the subbands of 2-phonon resonance mid-infrared quantum cascade laser. *Appl. Phys. Lett.* **101**(6), 061110 (2012). <https://doi.org/10.1063/1.4745013>
- Kubis, T., Yeh, C., Vogl, P., Benz, A., Fasching, G., Deutsch, C.: Theory of nonequilibrium quantum transport and energy dissipation in terahertz quantum cascade lasers. *Phys. Rev. B* **79**(19), 195323 (2009). <https://doi.org/10.1103/PhysRevB.79.195323>
- Lake, R., Klimeck, G., Bowen, R.C., Jovanovic, D.: Single and multiband modeling of quantum electron transport through layered semiconductor devices. *J. Appl. Phys.* **81**(12), 7845–7869 (1997). <https://doi.org/10.1063/1.365394>
- Lee, S.-C., Wacker, A.: Nonequilibrium Green's function theory for transport and gain properties of quantum cascade structures. *Phys. Rev. B* **66**(24), 245314 (2002). <https://doi.org/10.1103/PhysRevB.66.245314>
- Steiger, S., Povolotskyi, M., Park, H.-H., Kubis, T., Klimeck, G.: NEMO5: a parallel multiscale nanoelectronics modeling tool. *IEEE Trans. Nanotechnol.* **10**(6), 1464–1474 (2011). <https://doi.org/10.1109/TNANO.2011.2166164>
- Terazzi, R., Faist, J.: A density matrix model of transport and radiation in quantum cascade lasers. *New J. Phys.* **12**(3), 033045 (2010). <https://doi.org/10.1088/1367-2630/12/3/033045>
- Van de Walle, ChG: Band lineups and deformation potentials in the model-solid theory. *Phys. Rev. B* **39**(3), 1871–1883 (1989). <https://doi.org/10.1103/PhysRevB.39.1871>
- Vurgaftman, I., Meyer, J.R., Ram-Mohan, L.R.: Band parameters for III–V compound semiconductors and their alloys. *J. Appl. Phys.* **89**(11), 5815–5875 (2001). <https://doi.org/10.1063/1.1368156>

Publisher's Note Springer Nature remains neutral with regard to jurisdictional claims in published maps and institutional affiliations.